
01 Jan 2015

Angiogenic Effect of Bioactive Borate Glass Microfibers and Beads in the Hairless Mouse

Richard J. Watters

Roger F. Brown

Missouri University of Science and Technology, rbrown@mst.edu

D. E. Day

Missouri University of Science and Technology, day@mst.edu

Follow this and additional works at: https://scholarsmine.mst.edu/biosci_facwork



Part of the [Biology Commons](#), and the [Ceramic Materials Commons](#)

Recommended Citation

R. J. Watters et al., "Angiogenic Effect of Bioactive Borate Glass Microfibers and Beads in the Hairless Mouse," *Biomedical Glasses*, vol. 1, no. 1, pp. 173-184, Walter de Gruyter GmbH, Jan 2015.

The definitive version is available at <https://doi.org/10.1515/bglass-2015-0017>



This work is licensed under a [Creative Commons Attribution-Noncommercial-No Derivative Works 3.0 License](#).

This Article - Journal is brought to you for free and open access by Scholars' Mine. It has been accepted for inclusion in Biological Sciences Faculty Research & Creative Works by an authorized administrator of Scholars' Mine. This work is protected by U. S. Copyright Law. Unauthorized use including reproduction for redistribution requires the permission of the copyright holder. For more information, please contact scholarsmine@mst.edu.

Research Article

Open Access

Richard J. Watters, Roger F. Brown*, and Delbert E. Day

Angiogenic Effect of Bioactive Borate Glass Microfibers and Beads in the Hairless Mouse*

DOI 10.1515/bglass-2015-0017

Received Oct 15, 2015; revised Nov 24, 2015; accepted Dec 05, 2015

Abstract: The purpose of this project was to investigate the angiogenic mechanism of bioactive borate glass for soft tissue repair in a ‘hairless’ SKH1 mouse model. Subcutaneous microvascular responses to bioactive glass microfibers (45S5, 13-93B3, and 13-93B3Cu) and bioactive glass beads (13-93, 13-93B3, and 13-93B3Cu) were assessed via: noninvasive imaging of skin microvasculature; histomorphometry of microvascular densities; and quantitative PCR measurements of mRNA expression of VEGF and FGF-2 cytokines. Live imaging via dorsal skin windows showed the formation at two weeks of a halo-like structure infused with microvessels surrounding implanted borate-based 13-93B3 and 13-93B3Cu glass beads, a response not observed with silicate-based 13-93 glass beads. Quantitative histomorphometry of tissues implanted with plugs of 45S5, 13-93B3, and 13-93B3Cu glass microfibers revealed microvascular densities that were 1.6-, 2.3-, and 2.7-times higher, respectively, than the sham control values whereas 13-93, 13-93B3, and 13-93B3Cu glass beads caused the microvascular density to increase 1.3-, 1.6-, and 2.5-fold, respectively, relative to sham controls. Quantitative PCR measurements indicate a marginally significant increased expression of VEGF mRNA in tissues with 13-93B3Cu glass beads, an outcome that supported the hypothesis that copper-doped borate glass could promote VEGF expression followed by angiogenesis for enhanced wound healing.

Keywords: Angiogenesis; copper-doped bioactive borate glass; bioactive glass microfibers; bioactive glass beads; *in vivo*, soft tissue

1 Introduction

Each year approximately 6.5 million people in the United States receive treatment for non-healing chronic skin wounds, a significant health care challenge that costs an estimated \$25 billion dollars annually [2]. Chronic skin wounds, wounds that do not heal within three months, consist of three primary types: venous ulcers, diabetic ulcers, and pressure ulcers [3]. Wounds of these types frequently become infected and gangrenous, often resulting in amputation and increased mortality [4]. Although the cause of impaired healing of chronic skin wounds remains unknown, there is compelling indirect evidence that neovascularization and angiogenesis have central roles in the healing of soft tissue wounds. This link has been established by numerous clinical observations of insufficient angiogenesis associated with non-healing chronic skin wounds [5–12]. As an example, non-healing diabetic foot ulcers appear to be an outcome of the diminished peripheral blood flow that is common to diabetic patients [13].


The finding that specific angiogenic cytokines are often deficient in patients with chronic wounds has prompted tests of various pro-angiogenic growth factors in experimental treatments of chronic wounds [14]. As an example, the pro-angiogenic growth factor platelet derived growth factor (PDGF) is the active component in the topical gel Becaplermin used in trial clinical treatment of lower extremity ulcers [15]. Other experimental treatments with promising results include the use of vascular endothelial growth factor A (VEGFA) and fibroblast growth factor B (bFGF or FGF2), both of which are known to promote angiogenesis [16, 17]. At present, PDGF is the only growth factor approved by the FDA for treating non-healing chronic wounds in humans [18].

A simpler and less expensive method for cytokine-induced angiogenesis might involve incorporation of pro-angiogenic ions in wound treatment materials. Ions such as copper, cobalt, boron, and zinc have been shown to

Richard J. Watters: Department of Biological Sciences and
²Graduate Center for Materials Research, Missouri University of
Science and Technology, Rolla, MO 65401

***Corresponding Author: Roger F. Brown:** Department of Biological Sciences, Missouri University of Science and Technology, Rolla, MO 65401; Email: rbrown@mst.edu

Delbert E. Day: Graduate Center for Materials Research Missouri University of Science and Technology

 © 2015 R. J. Watters *et al.*, published by De Gruyter Open.

This work is licensed under the Creative Commons Attribution-NonCommercial-NoDerivs 3.0 License.

* A preliminary report of the project was presented by Delbert E. Day at Glass & Optical Materials Division and Deutsche Glastechnische Gesellschaft Joint Annual Meeting, May 17-21, 2015, Miami, Florida, USA [1].

Table 1: Composition of bioactive glasses used for subdermal implantations (composition values listed as wt.%).

Glass	SiO ₂	B ₂ O ₃	Na ₂ O	CaO	MgO	K ₂ O	P ₂ O ₅	CuO
45S5	45.00	0	24.50	24.50	0	0	6.00	0
13-93	53.00	0	6.00	20.00	5.00	12.00	4.00	0
13-93B3	0	53.00	6.00	20.00	5.00	12.00	4.00	0
13-93B3Cu	0	52.79	5.98	19.92	4.98	11.95	3.98	0.40

have positive effects on angiogenesis [19, 20]. Dissolvable materials containing one or more of these pro-angiogenic ions could be effective vehicles for localized delivery of angiogenic ions. Dissolution products released from boron-doped 45S5 bioactive glass were recently reported to promote *in vitro* proliferation of endothelial cells [21] and *in vivo* angiogenesis [22]. Borate-based bioactive glass was recently tested as a delivery device for angiogenic ions in soft tissue repair [23]. Bioactive glass scaffolds doped with copper and other elements were subcutaneously implanted into laboratory rats and left for six weeks. Analysis of tissues implanted with scaffolds prepared from a borate-based glass designated 13-93B3 and 13-93B3 with 0.4% CuO showed a higher density of microvasculature than those with silica-based glass fiber scaffolds (although no sham control tissues were included for baseline comparison) [23]. Based on the promising outcome of the rodent study an initial clinical evaluation of the use of borate glass microfibers in wound healing was performed by the wound care unit at Phelps County Regional Medical Center (PCRMC). That study included 12 volunteers with chronic venous stasis wounds that were treated topically with repeated applications of microfibrillar dressings of 13-93B3 or 13-93B3Cu glass microfibers. Both of the two glasses accelerated the healing of previously unresponsive dermal wounds with complete healing of chronic wounds in 8 of the 12 patients in the clinical study. Empirical observations by the hospital staff showed that the 13-93B3 glass appeared to promote re-epithelialization while 13-93B3Cu microfibers appeared to promote granulation in wound healing [24]. A follow-up quantitative evaluation of the response of soft tissue to implants of borate-based microfibrillar glass was recently conducted in a rodent model [25]. Compressed mats of microfibrillar glass were subcutaneously implanted in Sprague Dawley rats and histologically evaluated at two, three, and four week intervals. Histomorphometric results indicated that borate-based microfibrillar glass doped with copper did promote angiogenesis.

This study was undertaken via three approaches to investigate the underlying mechanism of the angiogenic effect of bioactive borate glass using the SKH1 'hairless'

mouse as a model system. The first approach, pursued at the macroscopic level, involved real-time imaging of localized tissue responses to bioactive glass in dorsal skin fold preparations. The second approach involved histomorphometric assessment of the microvascular response to bioactive borate glass in excised subdermal tissues. The third and final approach involved measurement of cytokine expression in subdermal tissues implanted with copper-doped borate glass. The results supported our basic hypothesis that 13-93B3Cu bioactive glass stimulates expression of the cytokine VEGF resulting in angiogenesis in the treated tissue.

2 Materials And Methods

2.1 Bioactive glass

Bioactive glass materials used in this study (provided by MO-SCI Inc, Rolla, MO) included two types of silica-based glasses, 45S5 glass and 13-93 glass, plus two borate-based glasses with the designations 13-93B3 and 13-93B3Cu. Compositions of these four glasses are provided in Table 1. The materials were used in two physical forms for implantation: plugs of compressed glass microfibers; and fused glass beads. Batched glass microfibers (10±0.5 mg) were compressed in a specially constructed teflon mold to form 2 mm diameter porous plugs (example shown in Figure 1A). Additional 10 mg±0.5 mg batches of the glass microfibers were placed in a graphite mold and each batch fused with a butane torch to create a smooth spherical bead (Figure 1B). The compressed glass microfiber plugs and glass beads were sterilized by dry heating overnight at 200°C prior to implantation.

2.2 Dorsal skin window frame

Special frames for viewing microvessels were fabricated from 0.45 mm thick aluminum stock using two 25 mm × 15 mm rectangular pieces to form one frame. Two 8 mm diameter windows were bored in each frame, the

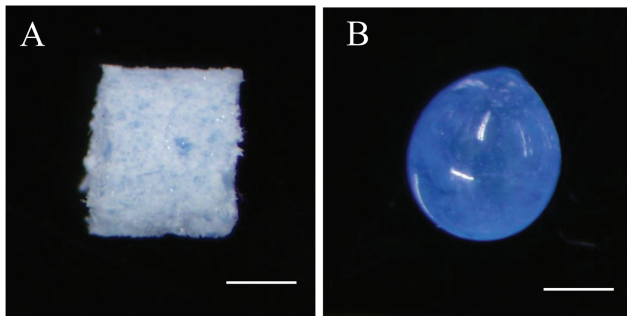


Figure 1: Two physical forms of the bioactive glass samples implanted in mice. (A) Compressed 2 mm diameter plugs of glass microfibers (side view); (B) fused 2 mm diameter glass bead. Both samples shown here are 13-93B3Cu glass (hence blue color). Scale bar represents 1.0 mm.



Figure 2: Installed skin window frame on SKH1 mouse immediately after surgical implantation of fused glass beads (raised area in each window).

edges were smoothed, and five 1.5 mm holes added along the perimeter for suturing the frame to the dorsum of the mouse.

2.3 Animals

All experiments were performed with female 5 to 7 week old SKH1 mice (24±4 g). This murine strain was chosen because of its hairless trait, a feature that facilitates the trans-illuminated viewing of skin microvessels. NIH guidelines for the care and use of laboratory animals (NIH Publication #85-23 Rev. 1985) were followed.

2.4 Surgical procedures

Each of two replicate experiments for real-time microvascular imaging and histomorphometric assessment included four treatment groups with three animals per group. Test animals were anesthetized by intraperitoneal injection of a ketamine/xylazine/acepromazine mixture and the dorsal surface disinfected with Betadine surgical scrub. The prepped animal was placed on a temperature-controlled stainless steel surgical platform and a fold of dorsal skin was lifted and centered. Two 3 mm incisions were made along the mid-sagittal axis in the dorsal skin fold approximately 16 mm apart and a subdermal pocket formed at each incision. After pipetting 3 μ l of phosphate buffered saline (PBS) into the incision to act as lubricant, a sterile 1.5 mm diameter stainless steel rod was used to gently push either a glass plug or a glass bead approximately 8 mm into the subdermal pocket and the incision then closed using a minimal amount of cyanoacrylate adhesive. Following implantation of the bioactive glass samples, a pre-sterilized frame was positioned such that the implants were approximately in the middle of each of the two windows as shown in Figure 2. The two sides of the dorsal skin window frame were sutured together with Ethicon 4-0 black nylon monofilament followed by subcutaneous injection of Ketofen analgesia for post-surgical pain management. There were no losses due to infection. A final experiment performed for measurement of cytokine expression included four treatment groups with three animals per group. A single 3 mm incision was created along the dorsal midline and a blunt probe was used to form two contralateral subdermal pockets. Two bioactive glass beads were separately placed in the incision, gently guided into a subdermal pocket, and the incision closed with a minimal amount of cyanoacrylate adhesive.

2.5 Dorsal skin window imaging

To begin the imaging, an alert animal was secured in a tubular restraint device and then placed on a plexiglass viewing platform with the animal positioned on its side. A fiber optic light source mounted below the platform was adjusted to project light through the skin enclosed in the window frame. The 10x macrozoom lens of a digital camera mounted on a boom stand above the platform was adjusted to bring the trans-illuminated skin fold into focus and digital images of the tissue were collected.

2.6 Tissue collection and processing for histology

At three weeks post-implantation, animals were euthanized by CO₂ inhalation. Each implantation site (bead or plug) was excised with an 8 mm biopsy punch (Miltex) and immediately placed in 10% neutral buffered formalin for four days. Fixed tissue samples were rinsed twice in PBS two times, dehydrated in a vacuum infiltration tissue processor (TissueTek 2000), and embedded in paraffin. Tissue blocks were sectioned at 5 µm and mounted on positively charged microscope slides.

2.7 Staining and Histomorphometry

Mounted sections of subdermis were stained using Periodic Acid Schiff (PAS) solution followed by a 1% light green counterstain. This sequence caused the endothelial basal lamina to stain dark blue by the PAS solution while erythrocytes were stained green by the 1% light green counterstain thereby facilitating visualization of the microvasculature [26]. Stained tissue sections were examined under an Olympus BX53 microscope fitted with an Olympus DP70 digital camera. Using the 4× objective, the entire tissue section was scanned, digitally photographed, and the 4× photos ‘photomerged’ to form a single composite image. Each composite image was then overlaid with a numbered grid that was sized such that each individual box of the grid corresponded to the area of one 20× field (as shown in Figure 3). Continuing with the 4× objective, the boxes of

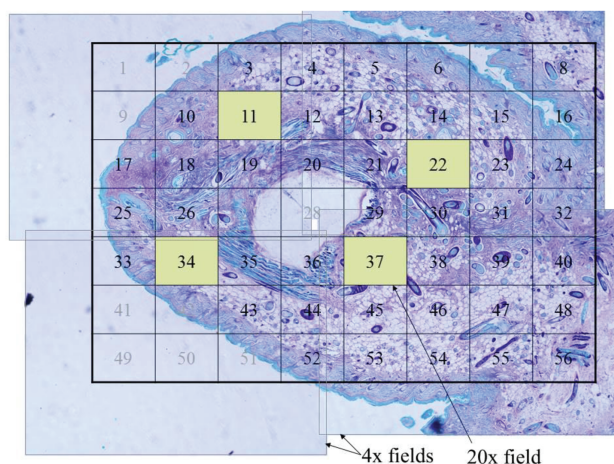


Figure 3: Steps of randomly selecting 20× fields for quantification. A grid overlay scaled such that each box represents a 20× field was placed on a composite image of PAS-stained tissue followed by randomized selection of four of the qualified fields for quantification.

the grid were examined to identify ‘qualified’ fields, which were those in which subdermis comprised 50% or more of the area within the box. Using the random number generator function of Microsoft Excel®, four of the ‘qualified’ fields were randomly selected for detailed histological examination under the 20× objective to identify and encircle microvessels. ImageJ software was then used for histomorphometric evaluation of microvessel density via the following equation where void area is area devoid of tissue:

$$\% \text{Vessel area} = \left(\frac{\text{Vessel Area}}{\text{Total Area} - \text{Void Area}} \right) \times 100$$

2.8 Extraction of total RNA

Immediately following euthanasia, whole skin at the implant site was excised with an 8 mm biopsy punch and snap frozen in liquid nitrogen. Each implanted treatment bead or plug was carefully removed and the frozen tissue then pulverized under liquid nitrogen using a pre-chilled mortar and pestle. TRIzol® reagent was used to isolate total RNA via a modified procedure of Chomczynski & Sacchi [27, 28]. The gel-like RNA pellet was washed twice in RNase-free ethanol, partially dehydrated, and suspended in 40 µl diethylpyrocarbonate (DEPC) treated water. The quantity of total RNA recovered was determined from 260 nm and 280 nm absorbance measurements with a Nanodrop 3000 spectrophotometer. To assess RNA quality, an aliquot of total RNA (1 µg) was run on a 1% agarose/formaldehyde denaturing gel and the gel then stained with SYBR-Gold nucleic acid stain for visualization of the sharpness of 18S and 28S bands with absence of smearing.

2.9 Analysis of gene expression by quantitative PCR

Analysis of gene expression by quantitative PCR (qPCR) was performed on a fee basis by the Mouse Biology Program at the University of California-Davis. The one, two, and three week RNA samples from sham control and the 13-93B3Cu treated tissues were converted to complementary DNA (cDNA) and custom constructed oligonucleotide probes (TaqMan® probes) specific for the VEGF and FGF-2 genes were synthesized plus a probe for the GAPDH gene which was used as an endogenous control. As product cDNA was amplified during thermal cycling, the TaqMan® probe for each cytokine was degraded and a fluorescent signal eventually detected by the fluorescence sensor of

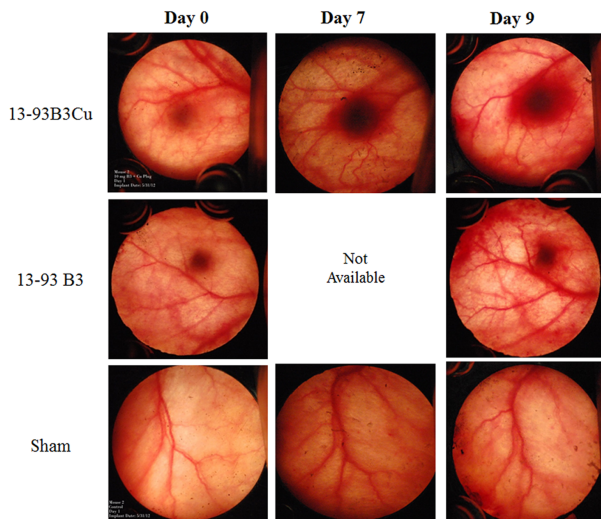


Figure 4: Skin window imaging of tissue responses to microfibrinous plugs. Photos show nine day progression of responses to 13-93B3 and 13-93B3Cu microfibrinous plugs compared to a sham implant control.

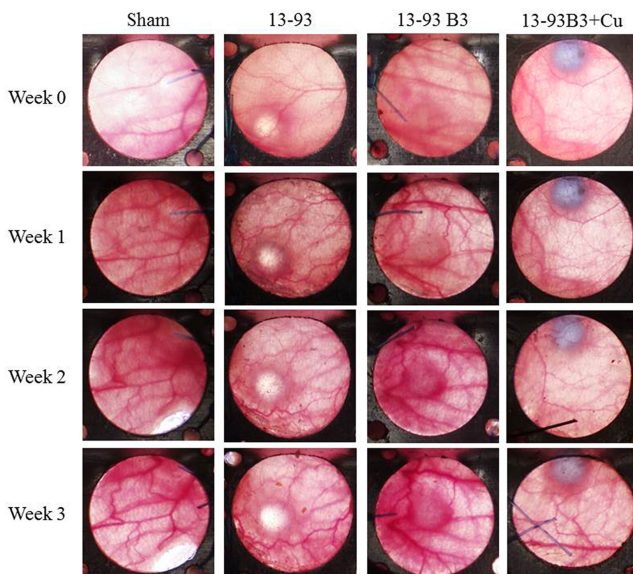


Figure 5: Skin window imaging of tissue responses to glass beads. Photos show three week progression of responses to 13-93, 13-93B3, and 13-93B3Cu glass beads compared to a sham implant control.

the instrument. The thermal cycle at which the concentration of amplified product cDNA reached the detection threshold (designated Ct, the threshold cycle) was used as a measurement endpoint of the assay [29]. The levels of expression of target genes were normalized to the GAPDH endogenous control by subtracting the control Ct value from the target gene Ct to obtain ΔCt values [30]. Comparisons between treatment groups of relative expression of a tar-

get gene was determined by delta-delta Ct calculation [30] where $2^{(-\Delta\Delta Ct)}$ represents the relative fold difference between target gene expression in a treated tissue sample compared to the same target gene in a sham control sample.

2.10 Statistical analysis

Data sets are presented as means \pm standard error of the mean. Evaluation of treatment groups from experiments was done by one way analysis of variance (ANOVA) followed by the Tukey post-hoc test to identify significant differences between treatment groups. Differences between groups were considered significant with p -values less than 0.05 ($p < 0.05$) and marginally significant with p -values less than 0.10 ($p < 0.10$).

3 Results

3.1 Imaging of localized tissue response to bioactive glass implants

The materials initially used for live imaging of localized tissue responses were compressed plugs of glass microfibrers. Successful imaging of implants for two or more weeks was possible with fewer than 30% of the microfibrinous glass plugs. Examples of responses that were successfully imaged in those tissues are presented in Figure 4. The images in this figure show a nine day progression of tissue responses to implanted plugs of borate based 13-93B3 and 13-93B3Cu microfibrers compared to a sham implant control. Day zero pictures were taken within 30 minutes after implantation of the test materials. Minor edema was observed in the tissue surrounding the 13-93B3Cu plug although the edema subsided prior to the subsequent day 7 picture. The day 7 photo shows a halo response beginning to develop around the 13-93B3Cu plug extending approximately 1 mm beyond the periphery of the implant. At day 9, the 13-93B3Cu plug was encircled by a prominent halo response that was approximately 5 mm in diameter and qualitatively more pronounced than at day 7. As shown in the figure, a minor halo response was visible encircling the 13-93B3 plug at day 9. The tissue at the sham implant control site remained unchanged during the course of the nine day observation period with no visible halo development. In contrast to the samples shown here, many of the other microfibrinous plug implants were within a few days surrounded by erythema and mild edema, early phase in-

Table 2: Qualitative evaluation of soft tissue response to beads implanted in dorsal skin.

Implant interval	Bead type	Beads (shams) implanted	Beads (shams) remaining	Fraction with halo	Halo density*
1 wk	none (Sham)	(5)	(4)	0/4	0
	13-93	5	5	0/5	0
	13-93B3	5	5	0/5	0
	13-93B3Cu	5	4	1/4	+
2 wk	none (Sham)	(5)	(4)	0/4	0
	13-93	5	5	0/5	0
	13-93B3	5	5	3/5	++
	13-93B3Cu	5	4	3/4	++
3 wk	none (Sham)	(5)	(3)	0/3	0
	13-93	5	5	1/5	+
	13-93B3	5	5	3/5	++
	13-93B3Cu	5	3	2/3	++/+++

* Key to qualitative assessment of halo density:
 No halo observed
 Minor redness surrounding glass bead
 Complete halo surrounding glass bead
 Intense halo surrounding bead

flammatory responses that obscured direct tissue imaging. To reduce the inflammatory response artifact, spherical beads of fused glass were adopted for subsequent implantations. The rationale for switching to spherical beads was the premise that the smooth surface of the beads would be less irritating than compressed microfibers, many of which have exposed ends that could cause tissue irritation.

Representative live macroscopic images of localized tissue responses to bioactive glass beads implanted in dorsal skin window preparations and subsequently photographed at one, two and three weeks after implantation are shown in Figure 5. The week zero skin window photos show minor inflammation that formed quickly around the 13-93 and 13-93B3 beads. This minor inflammation appeared to subside before the follow-up week one photos were taken. One week post implantation there was little or no observable response with any of the implanted beads or sham control implantations except for minor redness surrounding one of the implanted 13-93B3Cu beads and one 13-93B3 bead. Tissue response at week 2 shows a halo-like body surrounding a 13-93B3 and 13-93B3Cu bead. The halos around the beads at week 2 extended approximately 1 mm beyond the edge of the bead, a finding also observed with the other borate beads that were implanted. Another interesting morphological feature observed in the week 2 images is an increasing prominence of the large

vessels near the 13-93B3 bead. There were no discernable changes in appearance of the sham control tissues during the three week observation period. There was a discernable difference between the borate based 13-93B3 and 13-93B3Cu beads and the silicate based 13-93 glass beads at week 3. The borate-based 13-93B3 bead had a distinct and localized halo response around the implant. In contrast, the silicate-based 13-93 glass beads produced little or no discernable halo response. Qualitative evaluations of soft tissue response to beads are presented in Table 2. As indicated in the table, a distinct halo-like body was observed around only one of the five 13-93 silicate glass beads at week 3. In contrast, distinct halos were observed at week 3 around three of the five implanted 13-93B3 beads and two of the three remaining 13-93B3Cu beads. The halos surrounding the borate-based 13-93B3 and 13-93B3Cu beads had an outer diameter of approximately 3–4 mm, became prominent at week two, and remained distinct until the animals were sacrificed at week three. Overall, the outcome of the live imaging was the finding of essentially no new vessels nor increased microvascular density visible in tissue surrounding the 13-93 glass beads while tissues implanted with the borate-based 13-93B3 and 13-93B3Cu beads showed consistent halo formation around the implanted bead.

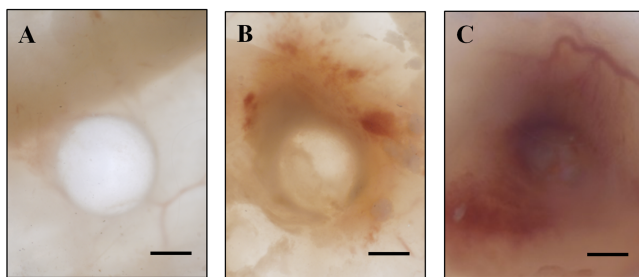


Figure 6: Representative 3 week photo images of tissue response to beads implanted subdermally without skin window frames. Tissues were photographed from the subdermal side rather than by indirect viewing through the skin from the epidermal side. The glass beads implanted were: (A) 13-93; (B) 13-93B3; and (C) 13-93B3Cu. Scale bar represents 1 mm.

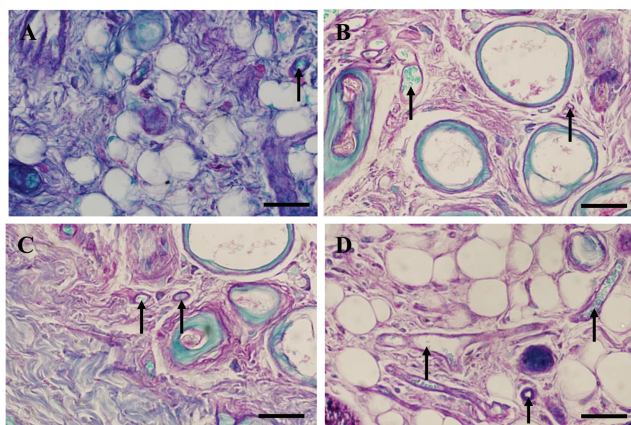


Figure 7: Representative 20× photo images of PAS-stained sections of tissue recovered after 3 weeks from subcutaneous sites of implantation of bioactive glass microfibers. The types of microfibers implanted were: (A) none (sham control); (B) 45S5 (C) 13-93B3; and (D) 13-93B3Cu. Arrows point to some of the microvessels seen in the tissues. Scale bar represents 50 μm.

A follow-up ancillary experiment was conducted to further characterize the halo structures. The follow-up included a separate group of 10 SKH1 mice that received subdermal implantations of 13-93, 13-93B3, and 13-93B3Cu fused beads without the use of the skin window frames. The objective was direct imaging of subdermal microvascular responses by photoimaging the subdermis of necropsied skin rather than by indirect viewing of subdermal microvascular responses from the epidermal side of intact live skin enclosed within the dorsal skin window preparations. Three weeks after implantation, the animals were euthanized and the skin reflected for macroscopic photo imaging of the subdermal soft tissue. Three of the four sham implantation sites were no longer detectable when the subdermal surface of the necropsied skin was examined whereas at the one sham site that was still some-

what discernable there was only a very small (< 1 mm diameter), slightly reddish body. The outcome with the beads, as shown by the representative images in Figure 6, was the finding of a reddish, halo-like structure surrounding each of the four implanted 13-93B3Cu beads and each of the four implanted 13-93B3 beads but no similar halo-like structure at any of the four sites with 13-93 beads. As shown, the halo-like structures surrounding the 13-93B3Cu beads were more intense than the halos surrounding the 13-93B3 beads. Furthermore, the halo structures around 13-93B3Cu beads were about 4 mm in diameter, similar to the size of the halo-like structures observed in the live dorsal skin window preparations. The physical appearance of the implant was also observed. At three weeks post implantation the glass beads were intact, appeared to be the same diameter as when initially implanted, and had no noticeable reacted layer on their surface.

3.2 Sample recovery and histological evaluation of soft tissue response

At conclusion of the three week implantation, discs of whole skin were excised from the dorsal skin fold preparations and the implants quickly examined. The microfiber plugs appeared approximately the same size at three weeks post-implantation but were covered with a thin white reacted layer. In addition, the plugs were soft, moist, and crumbled upon removal. The glass beads appeared the same diameter as when implanted, remained intact upon removal, and had no discernable reactive layer on their surface. After processing and staining, the entire area of each tissue section was initially scanned under a 4× objective and composite 4× images prepared. Many of these tissue sections had a central void area that corresponded to the site of implantation of the test glass sample.

The four panels of Figure 7 show representative 20× images of PAS-stained sections of subdermal tissues removed three weeks after implantation of glass microfiber plugs. Figure 7A, an example of subdermis observed in necropsied tissues from sham control implant sites, shows adipose and areolar tissues with a low microvascular density. The image in Figure 7B is a representative example of tissue implanted with silicate-based 45S5 glass microfibers. The section shown here has a tissue composition similar to that of the sham control sample plus a similar microvessel density. Moderate amounts of fibrous tissue were observed in the tissue samples from the sites of implantation of 13-93B3 and 13-93B3Cu glass microfibers

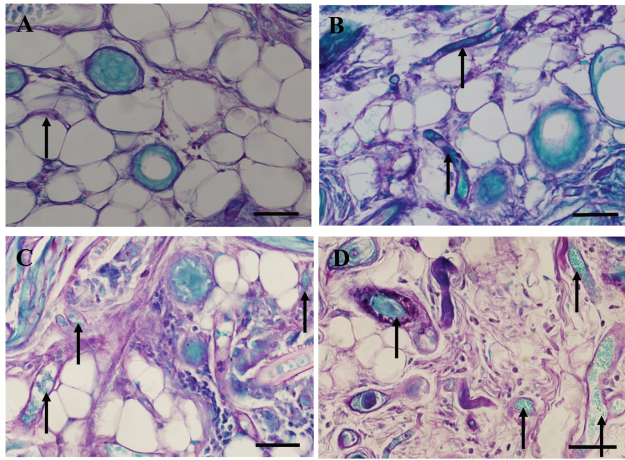


Figure 8: Representative 20× photo images of PAS-stained sections of tissue recovered after 3 weeks from subcutaneous sites of implantation of fused bioactive glass beads. The types of glass beads implanted were: (A) none (sham control); (B) 1393 glass; (C) 13-93B3 glass; and (D) 13-93B3Cu. Arrows point to some of the microvessels seen in the tissues. Scale bar represents 50 μm.

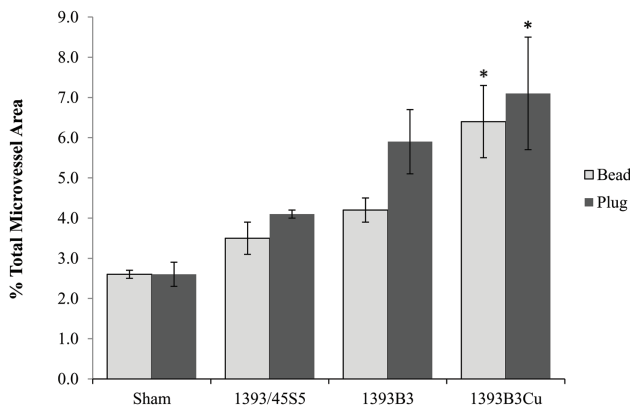


Figure 9: Comparison of microvessel densities three weeks post-implantation in response to fused bioactive glass beads and microfibrous plugs. Values are means ± SEM for five replicates with each material. Asterisks (*) identify group means significantly different from sham control at $p < 0.05$.

(shown in Figures 7C and 7D, respectively). The tissues from implants sites with the 13-93B3Cu glass qualitatively appeared to contain the highest density of microvessels of the four treatment groups.

The four panels of Figure 8 show representative 20× images of PAS-stained sections of subdermal tissues in skin samples removed three weeks after implantation of fused glass beads. The sham control sample in Figure 8A, which is representative of skin samples from other sham implant sites, shows adipose and areolar tissues with a low microvascular density. The image in Figure 8B, a rep-

resentative example of skin tissue samples from sites with the silicate 13-93 glass bead, shows tissue with a microvascular density similar to that of the sham control tissue. Somewhat higher amounts of fibrous tissue were observed in tissue sections from the 13-93B3 and 13-93B3Cu implantation sites (Figures 8C and 8D, respectively), a finding seen in other tissue samples with the borate glass beads. The microvasculature density appeared qualitatively higher in tissue with the borate-based 13-93B3 bead (Figure 8C) and higher yet in tissue with the 13-93B3 Cu bead (Figure 8D). Replicate tissue samples from the other sites of implantation of 13-93B3Cu glass beads also appeared qualitatively to have the highest density of microvessels. Many of the small microvessels visible in Figure 8D appear approximately the same diameter as an erythrocyte indicating that they are capillaries. The histological evaluation revealed that the replicate tissue samples recovered from the other sites of implantation of 13-93B3Cu glass beads also appeared qualitatively to have the highest density of microvessels.

3.3 Quantitative histomorphometry

A comparison of the microvessel density in soft tissue at the sites of implantation of bioactive glass beads and glass microfiber plugs is presented graphically in the bar chart of Figure 9. The total vessel areas observed in the two groups of sham control tissues were both calculated to be 2.6% of the total observed tissue area. Implantation of the fused glass beads and glass microfiber plugs resulted in the same overall trend for the tissue microvessel densities which were observed to be: lowest in the sham control tissues; slightly higher in tissues with silicate-based 13-93 or 45S5 glass; higher yet in tissues with 13-93B3 glass beads and glass microfiber plugs; followed by the highest microvessel densities in tissues implanted with 13-93B3Cu glass beads and glass microfiber plugs. The tissues implanted with the 13-93, 13-93B3, and 13-93B3Cu glass beads showed 33%, 58%, and 145% higher microvessel density values relative to the three-week sham control tissues, respectively. In a similar manner, the tissues containing 45S5, 13-93B3, and 13-93B3Cu glass microfiber plugs were found to have microvessel densities that were 56%, 124%, and 171% higher, respectively, compared to the three week sham control tissues. Results of the ANOVA test revealed the differences between the mean values of the various groups were greater than would be expected by chance and significant at the $p < 0.05$ level. The Tukey post-hoc test indicated that the higher microvessel densities of soft tissues with 13-93B3Cu glass beads or glass

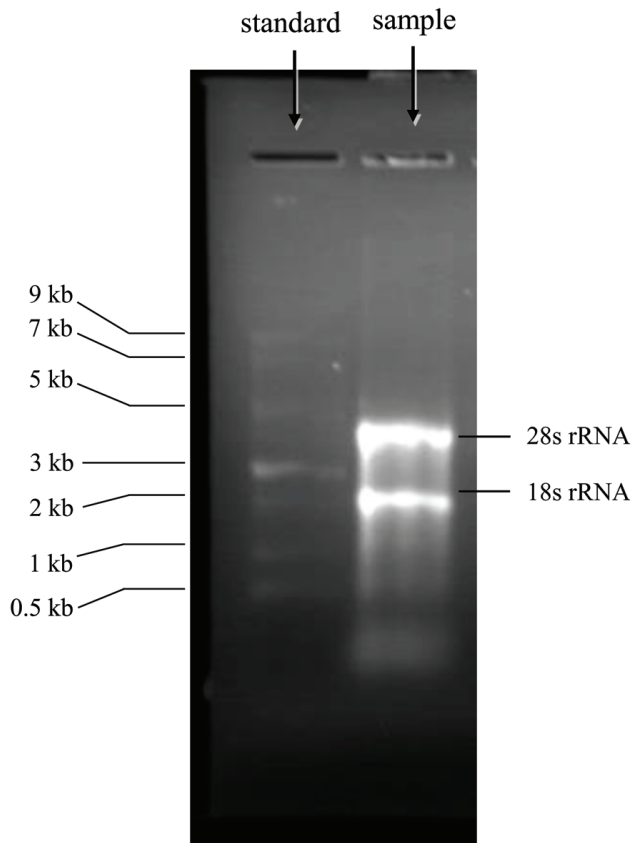


Figure 10: Agarose gel banding patterns of total RNA extract from a sham control tissue compared with a ladder standard. Bright bands in gel lane with the sample extract denote positions of 28S and 18S ribosomal RNA.

microfiber plugs compared to the microvessel densities of the sham control tissues was statistically significant at the $p < 0.05$ level. The higher microvessel densities of tissues implanted with 13-93B3 glass beads and 13-93B3 glass microfiber plugs compared to those in the sham control tissues were found to be marginally significant at the $p < 0.10$ level. In contrast, the microvessel densities of tissues with silicate-based 45S5 and 13-93 glass beads and glass microfiber plugs were not found to be statistically different from those of the sham control tissues.

3.4 Analyses of total RNA extracts

The yields of total RNA extracted from the frozen skin samples ranged from 120 ng/ μ l to 276 ng/ μ l for aliquots suspended in DEPC-treated water. The average A260/280 ratios measured for the extracts of total RNA from the frozen skin samples ranged from 1.82 to 1.88, values consistent with good quality RNA [31]. A representative example of

Table 3: Quantitative PCR measurements of cytokine gene expression in skin tissues with sham or borate bead implants. The Δ Ct values represent differences between target gene and endogenous control gene expression; each Δ Ct value is a mean \pm SEM for three replicate tissue samples. The $2^{(-\Delta\Delta Ct)}$ values represent fold changes of target gene expression relative to sham control.

Target gene	Bead type implanted	Implant duration (weeks)	Mean Δ Ct n = 3	$2^{(-\Delta\Delta Ct)}$ value
FGF2	none (Sham)	2	8.4 \pm 0.3	1.0
	13-93B3Cu	1	9.3 \pm 0.3	0.5
	13-93B3Cu	2	8.5 \pm 0.3	0.8
	13-93B3Cu	3	8.4 \pm 0.3	0.9
VEGF	none (Sham)	2	4.8 \pm 0.2	1.0
	13-93B3Cu	1	5.2 \pm 0.2	0.8
	13-93B3Cu	2	4.7 \pm 0.1	1.1
	13-93B3Cu	3	4.0 \pm 0.3*	1.8

* Group mean marginally different from sham control at $p < 0.10$.

the typical banding pattern seen after electrophoresis of the total RNA samples on 1% agarose/formaldehyde denaturing gel followed by SYBR-Gold staining is shown in Figure 10. Loaded in one lane of the gel was 1 μ g of total RNA from a sham control sample and in the adjacent lane an aliquot of a 500–9,000 base oligonucleotide ladder standard. The sample lane shows two intense bands at approximately 5 kb and 1.9 kb which correspond to 28S rRNA and 18S rRNA, respectively. Another important point was the near absence of smearing in the lane loaded with the sample extract RNA. A similar pattern of sharp 18S and 28S bands with nearly complete absence of smearing was seen in the gels run with all of the other preparations of total RNA extracted from frozen skin samples, findings that confirm the integrity of the RNA preparations.

3.5 qPCR analysis of gene expression

The qPCR assays of gene expression were performed on twelve RNA samples that included three samples of sham control RNA plus three samples each of RNA from tissues implanted with 13-93B3Cu glass beads for one, two, and three weeks. The results obtained are presented in Table 3 as Δ Ct values and as $2^{(-\Delta\Delta Ct)}$ values. The Δ Ct values represent expression of the FGF-2 and VEGF target genes normalized to the GAPDH endogenous control gene in the

sham and bead implanted tissues. The statistical analyses of the ΔCt mean values revealed a marginally significant difference at the $p < 0.10$ level ($p = 0.057$) between the levels of VEGF gene expression in tissues implanted with 13-93B3Cu glass beads for three weeks and the sham control tissues. There were no differences, however, between the levels of FGF-2 gene expression in the glass bead-implanted tissues and the sham control tissues. The last $2^{(-\Delta\Delta\text{Ct})}$ value listed in Table 3 indicates the level of VEGF expression was approximately 1.8 fold higher in tissue with 13-93B3Cu glass beads for three weeks compared with the level of VEGF expression in the sham control tissues.

4 Discussion

The common procedures and materials currently used for wound treatment often yield poor outcomes with chronic skin wounds, a major health care challenge. In that sense, the positive outcome of a recent clinical study at Phelps County Regional Medical Center (PCRMC) in Missouri is a noteworthy exception. This new procedure involved treatment of venous stasis wounds with dressings composed of borate-based glass microfibers [24]. The results of the PCRMC clinical trial revealed a dramatic improvement in the healing of previously non-responsive wounds for most of the volunteers enrolled in the study. Although these results were very encouraging, the mode of action of borate-based glass microfiber in wound healing was not addressed. Two separate follow-up investigations with rat models provided compelling evidence of an angiogenic effect of bioactive borate-based glass materials [23, 25].

This project was undertaken with the hairless mouse to specifically address the physiological and molecular mechanisms of the angiogenic effect of borate-based glass materials. The trans-illuminated skin window preparations were used with the anticipation they would allow clear delineation of microvessels. However, the high level of resolution needed for quantitative histomorphometry was not uniformly attained. But, the skin window imaging did allow a consistent qualitative distinction between the soft tissue responses to borate-based and silicate-based glass beads. As described in the Results section, much of the live soft tissue response observed around the borate-based beads involved the formation of a halo-like body. In the images with sufficiently high resolution, the halo bodies were recognized to be tissue clusters infused with microvessels. The formation of microvessel clusters or halo bodies observed around the 13-93B3 and 13-93B3Cu beads

is also consistent with the granulation tissue repeatedly observed in the PCRMC clinical study [24].

The conclusion that the halo observed around borate-based implants in skin window preparations was microvessel-rich soft tissue is supported by the subdermis necropsy images obtained in the ancillary experiment. In those necropsy images, very clearly delineated microvessels were visible within the reddish mass observed around the implanted borate-based glass beads. The reddish mass encircling the borate-based glass beads in the necropsy samples was also of similar diameter as the halo bodies observed in live imaging with skin window preparations. In addition, the halo body appeared most prominently around 13-93B3Cu glass bead and was virtually absent with the silicate-based 13-93 glass beads. The necropsy samples also showed microvessels ‘budding’ toward some of the 13-93B3Cu glass bead, an indication of angiogenesis.

The histological evaluation of the PAS-stained tissue sections also supported the interpretation that the halo bodies surrounding the borate glass beads were tissue clusters infused with microvessels. The microvessel densities observed in the stained histological sections were found to be higher within about a millimeter of the implanted borate bead compared to areas more distal to the bead. This finding also agrees with the higher microvessel densities observed within about a millimeter of subcutaneously implanted 13-93B3Cu glass microfibers as reported in the study by Lin and colleagues [25]. A recent study by Zhao and colleagues also reported evidence of prominent microvessel growth in full thickness skin defects in rodents treated with 13-93B3Cu glass microfibers [32]. It may be noted that the bioactive borate glass used in the latter study contained 3.0 wt% CuO compared to 0.4 wt% CuO in the 13-93B3Cu glass used in this investigation.

The histomorphometry results revealed higher microvessel densities around the microfibrillar plug than the fused glass bead. This difference may in part be attributable to the difference in the surface area of the two physical forms of the glass implants. The borate glass microfiber plugs have a much higher surface area than the 2 mm diameter glass beads. The borate glass microfibers with nominal diameters of approximately 2–5 μm have been shown to undergo complete reaction in three weeks releasing all of their boron and copper content [21]. The glass bead appeared to have no reacted surface layer, an indication of much slower dissolution. The glass microfiber plugs also had high porosity, another factor that would contribute to fast dissolution resulting in elevated localized concentrations of the angiogenic ions borate and copper [6, 33–35].

The microvessel densities observed in this study in response to implantation of the borate glass plugs and beads were about 30% less than the microvessel density values reported in the previous study by Lin and colleagues [25]. This difference may in part reflect differences in the method of random selection of areas in the stained slides for enumeration of microvessel densities. The method used in the previous study [25] involved unbiased selection of four areas that were all within approximately one millimeter from the implant site. The method used in this project involved randomly selecting four fields from a grid overlay on the entire tissue section which included areas that were a few millimeters from the implant site. The calculated average microvessel density value would be lessened by inclusion of areas for enumeration somewhat distal to the implant.

The effects of borate-based bioactive glass on expression of vascular endothelial growth factor (VEGF) *in vivo* had not been investigated prior to this study. Thus, an important and novel aspect of this investigation is the finding that skin tissue implanted with a 13-93B3Cu glass bead for three weeks exhibited elevated expression of VEGF mRNA, potentially triggering elevated VEGF, a growth factor with an essential role in wound healing [36]. Fibroblast growth factor-2 (FGF-2) has also been reported to be important in vasculogenesis [37]. However, the results of this study did not indicate increased expression of FGF-2 mRNA in response to the 13-93B3Cu glass beads. The relatively modest 1.8-fold increase in VEGF expression after three weeks in response to the 13-93B3Cu beads may be related to the slow dissolution of the glass beads. Higher levels of VEGF expression might be anticipated in response to implantation of more rapidly dissolving 13-93B3Cu glass microfibers.

The results of this project provide additional evidence that the borate-based bioactive glass beads and microfiber plugs promote angiogenesis, an essential step in wound healing. In addition, these positive results provide evidence that these materials are potentially useful for treating chronic non-healing wounds. An important outcome was the finding that copper-doped 13-93B3Cu glass is able to stimulate VEGF expression, thereby potentially triggering an angiogenic response. Collectively, these findings suggest bioactive borate glass would be a simple but effective vehicle for delivery of pro-angiogenic ions as an alternative to expensive growth factors for treatment for chronic wounds. Additional work is needed to determine if 13-93B3Cu glass microfibers would, by virtue of their high surface area, be more effective than the 13-93B3Cu glass beads in triggering expression of VEGF as well as other angiogenic cytokines in soft tissues.

Acknowledgement: This investigation was supported by funds from the Center for Biomedical Sciences and Engineering at Missouri University of Science and Technology. The bioactive glass materials used in this study were donated by the MO-Sci Corp in Rolla, MO.

References

- [1] Brown R., Watters R., Day D., Angiogenic Response of Bioactive Borate Glass Beads & Microfibers in “Hairless” Mice, The American Ceramic Society-Glass & Optical Materials Division and Deutsche Glastechnische Gesellschaft Joint Annual Meeting, Miami, FL, 17–21 May 2015.
- [2] Chandan S., Gordillo M., Sashwati R., Kirsner R., Lambert L., Hunt T.K., *et al.*, [Human skin wounds: a major and snowballing threat to public health and the economy](#), *Wound Repair Regen* 2009, 17, 763–771.
- [3] Wu S., Driver V., Wrobel J., Armstrong D., Foot ulcers in the diabetic patient, prevention and treatment, *Vasc Health Risk Manag* 2007, 3, 65–76.
- [4] Caputo G., Cavanagh P., Ulbrecht J., Gibbons G., Karchmer A., [Assessment and management of foot disease in patients with diabetes](#), *New Engl J Med* 1994, 13, 854–860.
- [5] Keshaw H., Forbes A., Day R., [Release of angiogenic growth factor from cells encapsulated in alginate beads with bioactive glass](#), *Biomaterials* 2005, 26, 4171–4179.
- [6] Barralet J., Gbureck U., Habibovic P., Vorndran E., Gerard C., Doillon C., [Angiogenesis in calcium phosphate scaffolds by inorganic copper ion release](#), *Tissue Eng* 2009, 15, 1601–1608.
- [7] Li J., Zhang Y., Kirsner R., Angiogenesis in wound repair: Angiogenic growth factors and the extracellular matrix, *Microsc Res Tech* 2003, 60, 107–114.
- [8] Cole R., Liu F., Herron B., Imaging of angiogenesis: past, present and future, In: A. Mendez – Vilas, J. Diaz (Eds.), *Microscopy: Science, Technology, Applications and Education*, Vol 3, Badajoz, Spain, 2010.
- [9] Folkman J., Shing Y., Angiogenesis, *J Biol Chem* 1992, 267, 10931–10934.
- [10] Shih S., Robinson G., Perruzzi C., Calvo A., Desai K., Green J., *et al.*, Molecular profiling of angiogenesis markers, *Am J Pathol* 2002, 161, 35–40.
- [11] Clayton W., Elasy T., A review of the pathophysiology, classification, and treatment of foot ulcers in diabetic patients, *Clin Diabetes* 2009, 27, 52–58.
- [12] Mohammad G., Pandey H., Tripathi K., Diabetic wound healing and its angiogenesis with special reference to nanoparticles, *Dig J Nanomater Bios* 2008, 3, 203–208.
- [13] Falanga V., Wound healing and its impairment in the diabetic foot, *Lancet* 2005, 366, 1736–43.
- [14] Demidova-Rice T., Durham J., Herman I., Wound healing angiogenesis: innovations and challenges in acute and chronic wound healing, *Adv Wound Care* 2012, 1, 17–22.
- [15] Papanas N., Efstratios M., Becaplermin gel in the treatment of diabetic neuropathic foot ulcers, *Clin Interv Aging*, Jun 2008, 3(2), 233–240.
- [16] Giavazzi R., Sennino B., Coltrini D., Garofalo A., Dossi R., Ronca R., *et al.*, Distinct role of fibroblast growth factor-2 and vascular

- endothelial growth factor on tumor growth and angiogenesis, *Am J Pathol* Jun 2003, 162, 1913–1926.
- [17] Witkowski J., Parish L., [Rational approach to wound care](#), *Int J Dermatol* 1992, 31, 27–28.
- [18] Fang R., Galiano R., A review of becaplermin gel in the treatment of diabetic neuropathic foot ulcers, *Biologics*, 2008, 2, 1–12.
- [19] Hoppe A., Mouriñob V., Boccaccini A., [Therapeutic inorganic ions in bioactive glasses to enhance bone formation and beyond](#), *Biomater Sci* 2013, 1, 254–256.
- [20] Chen Q., Zhu C., Thouas G., [Progress and challenges in biomaterials used for bone tissue engineering: bioactive glasses and elastomeric composites](#), *Prog Biomater* 2012, 1(1), 2.
- [21] Haro Durand L.A., Gongora A., Porto-Lopez J.M., Boccaccini A.R., Zago M.P., Baldi A., *et al.*, In vitro endothelial cell response to ionic dissolution products from a boron-doped bioactive glass in the SiO₂-CaO-P₂O₅-Na₂O system, *J Mater Chem B* 2014, 2, 7620–7630.
- [22] Haro Durand L.A., Vargas G.E., Romero N.M., Vera-Mesones R., Porto-Lopez J.M., Boccaccini A.R., *et al.*, Angiogenic effects of ionic dissolution products released from a boron-doped 45S5 bioactive glass, *J Mater Chem B* 2015, 3, 1142–1148.
- [23] Jung S., [Borate Based Bioactive Glass Scaffolds for Hard and Soft Tissue Engineering](#), Ph.D Dissertation, Missouri University of Science and Technology, Rolla, MO, 2010.
- [24] Taylor P., personal communication, Phelps County Regional Medical Center, Rolla, MO. 2012.
- [25] Lin Y., Brown R., Jung S., Day D., Angiogenic effects of borate glass microfibers in a rodent model, *J Biomed Mat Res A* 2014, 102(12), 4491–4499.
- [26] Eliza M., Ben I., Reuven B., Histopathological periodic acid-schiff stains of nail clippings as a second-line diagnostic tool in onychomycosis, *Am J Dermatopath* 2012, 34, 270–273.
- [27] Chomczynski P., Sacchi N., [Single-step method of RNA isolation by acid guanidinium thiocyanate-phenol-chloroform extraction](#), *Anal Biochem* 1987, 162, 156–9.
- [28] Chomczynski P., Sacchi N., [The single-step method of RNA isolation by acid guanidinium thiocyanate-phenol-chloroform extraction: twenty-something years on](#), *Nat Protoc* 2006, 1, 581–585.
- [29] Wong M., Medrano J., Real-time PCR for mRNA quantitation, *BioTechniques* 2005, 39, 75–85.
- [30] Livak K., Schmittgen T., Analysis of relative gene expression data using real-time quantitative PCR and the 2- $[\Delta\Delta Ct]$ method, *Methods* 2001, 25, 402–408.
- [31] Liu D., *Handbook of Nucleic Acid Purification*, CLC press, Boca Raton, FL. 2009.
- [32] Zhao S., Li L., Wang H., Zhang Y., Cheng X., Zhou N., *et al.*, [Wound dressings composed of copper-doped borate bioactive glass microfibers stimulate angiogenesis and heal full-thickness skin defects in a rodent model](#), *Biomaterials* 2015, 53, 379–391.
- [33] Kucan J., Robson M., Heggors J., Ko F., Comparison of silver sulfadiazine, povidone-iodine and physiologic saline in the treatment of chronic pressure ulcers, *J Am Geriatr Soc* 1981, 29, 232–235.
- [34] Harris E., [A requirement for copper in angiogenesis](#), *Nutr Rev* 2004, 62, 60–64.
- [35] Hu G., Copper stimulates proliferation of human endothelial cells under culture, *J Cellular Biochem* 1998, 69, 326–335.
- [36] Sen C.K., Copper-induced vascular endothelial growth factor expression and wound healing, *Am J Physiol* 2002, 282, H1821–H1827.
- [37] Emanuelli C., Madeddu P., Angiogenesis gene therapy to rescue ischemic tissues: achievements and future directions, *Brit J Pharmacol* 2001, 133, 951–958.